PHYSICAL REVIEW A, VOLUME 61, 041401(R)

Short-pulse chirped adiabatic population transfer in diatomic molecules

S. Kallush and Y. B. Band
Department of Chemistry, Ben-Gurion University of the Negev, Beer-Sheva, 84105, Israel
(Received 2 December 1999; published 28 February 2000)

Using the concept of light-induced potentials introduced by Garraway and Suominen [Phys. Rev. Lett. **80**, 932 (1998)], we study alternative schemes of adiabatic population transfer in a diatomic molecule from the lowest vibrational level of the ground electronic state to the lowest vibrational level of a third electronic state via allowed optical transitions from the ground and third electronic states to a second electronic state. Our chirped-pulse rapid adiabatic passage scheme is implemented with short-duration optical pulses, and can be understood in terms of ''road design engineering'' of the light-induced time-dependent adiabatic potential upon which the dynamics occurs. We explicitly show that complete adiabatic vibronic population transfer occurs using chirped picosecond-duration pulses in the sodium dimer example.

PACS number(s): 33.80.−b, 42.50.−p

Adiabatic passage between states of a three-level system via stimulated Raman adiabatic passage (STIRAP) using long pulse-duration optical pulses is by now a well-known technique for population transfer in atoms and molecules [1–12]. It might seem that this method cannot be used to move population in molecules from one vibronic state to another with intense short-duration optical pulses when the pulse-duration becomes comparable with or shorter than the vibrational (or rotational) period of the molecule ($\tau_{vib} \approx 200\times 10^{-15}$ s for Na_2). However, Garraway and Suominen [13] suggested that adiabatic wave-packet passage from the ground vibrational level of the ground electronic state to the ground vibrational level of a third electronic, having the same symmetry as the ground electronic state, can be implemented with short optical pulses when both ground and third electronic states are optically coupled with a second electronic state. Their method can be understood using the concept of adiabatic passage on light-induced time-dependent potentials. The order of the pulses in the pulse sequence adopted by Garraway and Suominen was the counterintuitive sequence familiar from STIRAP. Complete adiabatic transfer was implemented through the adiabatic eigenstate that smoothly goes from the ground state to the third state, while the second electronic state is not populated during the whole process.

Here we expand Garraway and Suominen's concept [13] and show that adiabatic passage on light-induced time-dependent potentials is an effective means of moving population in a controlled manner using other types of pulse sequences. Our method uses short-duration chirped optical pulses; an acronym for the method is chirped-pulse rapid adiabatic passage (CHIRAP). The pulse order need not be counterintuitive here; it can be intuitive or counterintuitive, depending upon whether the chirps are positive or negative, with the timing of the pulses not being the central issue. Our approach to determining the nature of the optical pulses necessary for complete controlled rapid adiabatic passage involves ''road design engineering'' of the light-induced time-dependent adiabatic potential; the wave packet for the system moves on the relevant adiabatic potential much as a school bus on a mountain road with an S curve that is properly banked. The quantities controlled and manipulated in the design problem are the pulse intensities, durations, relative timing, and chirp rates.

We explicitly consider a system similar to the sodium-dimer three-electronic-level model used by Garraway and Suominen, with transitions from the $X^1\Sigma_g^+$ ground state to the first excited $A^1\Sigma_u^+$ state, which is in turn coupled to the $1\,^1\Pi_g$ state (Garraway and Suominen used the $2\,^1\Pi_g$ state [13]). The object is to totally move the population from the ground vibrational level of $X^1\Sigma_g^+$, with a minimum in the potential at 5.8 bohr, to the ground vibrational level of the $1\,^1\Pi_g$ state, with a minimum in the potential at 9.0 bohr, by coupling these states to the $A^1\Sigma_u^+$ state, with a minimum in the potential at 6.8 bohr. The molecular potential parameters are taken from Refs. [14,15]. The electromagnetic field takes the form of short-duration light pulses with frequencies centered at ω_1 and ω_2, which are roughly resonant with the $X^1\Sigma_g^+ - A^1\Sigma_u^+$ and $A^1\Sigma_u^+ - 1^1\Pi_g$ transitions, respectively. The temporal duration of the pulses we have studied is from a fraction of a vibrational period up to many picoseconds. The two pulses can be temporally delayed, relative to one another, and chirped. Our use of chirped pulses is inspired by previous work [11,12] that demonstrated total adiabatic passage in a many-level system with long-pulse-duration chirped pulses (the dynamics there was independent in the vibrational coordinate R, because of the averaging over vibrational periods). The electric field can be written in the form $E(t)=[A_1(t)\exp(-i\omega_1 t)+\text{c.c.}]+[A_2(t)\exp(-i\omega_2 t)+\text{c.c.}]$, where the slowly varying envelope of each pulse, $A_k(t)$ $(k=1,2)$, is a complex function (in order to incorporate chirp) and turns on and then off in magnitude (i.e., rises from and falls to zero). The instantaneous frequency of pulse k takes the value of the central frequency ω_k at time $t=T_k$, and changes with time as $\omega_k(t)=\omega_k+(d\omega_k/dt)_{T_k}(t-T_k)+\cdots$. The peaks of the magnitude of the two pulses may be temporally displaced by $\Delta t \equiv t_1 - t_2$. We take the $A_k(t)$ to have the form

$$A_k(t)=A_{0k}\exp\left[-\frac{(t-t_k)^2}{2\sigma_k^2}-i\int^t dt'(\omega_k(t')-\omega_k)\right], \qquad (1)$$

where A_{0k} is the magnitude of the kth field component, t_k is the time at which it peaks, and σ_k is its temporal width. The form of the chirped frequency is taken as

$$\omega_k(t)=\omega_k+\delta\omega_k(1/\pi\ \arctan[(t-T_k)/\tau_k]), \tag{2}$$

where $\delta\omega_k$ is the frequency width of the chirp, T_k (not necessarily equal to t_k) is the time at which the frequency equals its central frequency ω_k, and τ_k is the temporal width of the chirp. It is convenient to define the Rabi frequencies $\Omega_k(t)$ that couple the molecular states, $\Omega_1(t)=\mu_{XA}A_1(t)/\hbar$ and $\Omega_2(t)=\mu_{A\Pi}A_2(t)/\hbar$. After making the rotating-wave approximation, the Hamiltonian for the molecule is

$$\mathbf{H}=-\frac{\hbar^2}{2m}\frac{\partial^2}{\partial R^2}\mathbf{1}+\mathbf{U}(R,t), \tag{3}$$

where $\mathbf{1}$ is the 3×3 unit matrix and $\mathbf{U}(R,t)$ is the electronic potential matrix, including the Rabi frequency coupling by the chirped time-dependent light fields,

$$\mathbf{U}(R,t)=\begin{pmatrix} U_X(R)+\hbar\Delta_1 & \hbar\Omega_1(t) & 0 \\ \hbar\Omega_1^*(t) & U_A(R) & \hbar\Omega_2(t) \\ 0 & \hbar\Omega_2^*(t) & U_\Pi(R)+\hbar\Delta_2 \end{pmatrix}. \tag{4}$$

Here U_i are the Born-Oppenheimer (BO) potentials for the $X^1\Sigma_g^+$, $A^1\Sigma_u^+$, and $1\,^1\Pi_g$ states, and Δ_k are the detunings of the pulses from resonance with the molecular transitions. The time-dependent couplings $\Omega_k(t)$ are taken to have smooth Gaussian magnitude and smooth chirps, thereby avoiding the complications arising in optimal control methods whose solution to the population transfer problem can involve extremely rapidly varying pulses.

By making a phase transformation to the wave function [11,12],

$$\begin{pmatrix} \Psi_1(t) \\ \Psi_2(t) \\ \Psi_3(t) \end{pmatrix}=\begin{pmatrix} \psi_1(t)\exp\left[-i\int^t dt'\,\omega_1(t')\right] \\ \psi_2(t) \\ \psi_3(t)\exp\left[-i\int^t dt'\,\omega_2(t')\right] \end{pmatrix}, \tag{5}$$

the potential-energy matrix can be written in the form

$$\tilde{\mathbf{U}}(R,t)=\begin{pmatrix} U_X(R)+\hbar(\Delta_1+\omega_1(t)-\omega_1) & \hbar|\Omega_1(t)| & 0 \\ \hbar|\Omega_1(t)| & U_A(R) & \hbar|\Omega_2(t)| \\ 0 & \hbar|\Omega_2(t)| & U_\Pi(R)+\hbar(\Delta_2+\omega_2(t)-\omega_2) \end{pmatrix}, \tag{6}$$

where now the off-diagonal matrix elements (the Rabi frequencies) are real, and therefore the Hamiltonian matrix is real-symmetric. The chirped frequencies now appear in the diagonal elements of the potential-energy matrix and the coupling between the potential surfaces occurs through the time-dependent Rabi frequency magnitudes $|\Omega_k(t)|$. In this basis, it can be seen that the chirps lower or raise the first $[\tilde{U}_{11}(R,t)]$ and third $[\tilde{U}_{33}(R,t)]$ diabatic potentials as a function of time, depending upon whether $\delta\omega_1$ and $\delta\omega_2$ are negative or positive (but do not influence the coupling terms between the surfaces). The chirp shape has been taken to be an arc-tangent function [Eq. (2)]. With $\delta\omega_1<0$, $\tilde{U}_{11}(R,t)$ decreases with time, while taking $\delta\omega_2>0$ in $\tilde{U}_{33}(R,t)$ yields a potential that increases with time [see Fig. 1(a)]. The intersection of the diabatic time-dependent surfaces depends on our choice of T_k and detunings Δ_k. For convenience, we take $\Delta_1=\Delta_2$, $t_1=t_2=0$, and $T_1=T_2=0$, so that the intersection of $\tilde{U}_{11}(R=0,t)$ and $\tilde{U}_{33}(R=0,t)$ occurs at $t=0$, while $\tilde{U}_{22}(R=0,t)$ is below this intersection at $t=0$. The parameters τ_k control the chirp durations. Increasing the τ's enhances the smoothness of the surfaces, which increases the region of proximity between them and prevents an undesired sharp intersection. The resultant three diabatic time-dependent surfaces $\tilde{U}_{jj}(R,t)$ [the diagonal elements of the matrix $\tilde{\mathbf{U}}(R,t)$ in Eq. (6) are plotted as a function of R and t in Fig. 1(a)]. The parameters used are $\hbar\Omega_k=0.004$ hartree, $\hbar\Delta_k=0.0015$ hartree, $T_k=t_k=0$ ps, $\sigma_k=5.2$ ps, and $\tau_k=12.2$ ps, for $k=1,2$, and $\hbar\delta\omega_1=-0.0173$ hartree, $\hbar\delta\omega_2=0.0484$ hartree.

Adiabatic surfaces $\epsilon_\alpha(R,t)$, $\alpha=1,2,3$ are obtained by diagonalizing the potential-energy matrix $\tilde{\mathbf{U}}(R,t)$ at each time t and coordinate R. These adiabatic surfaces are plotted as a function of R and t in Fig. 1(b). The highest adiabatic potential correlates with $X^1\Sigma_g^+$ at initial times and with $1\,^1\Pi_g$ at final times. Hence, as $t\to-\infty$, the highest-lying adiabatic surface correlates with the $\tilde{U}_{11}$ diabatic surface, whereas as $t\to\infty$, it correlates with the $\tilde{U}_{33}$ diabatic surface. This is different from the case considered by Garraway and Suominen where the adiabatic surface correlating with the initial and final electronic states is the middle adiabatic surface. In our case, the highest adiabatic surface contains a small admixture of the second electronic state, $A^1\Sigma_u^+$, for a short period of time. Consequently, the $A^1\Sigma_u^+$ state becomes populated for a short period of time during the dynamics, as described below. However, decay from the $A^1\Sigma_u^+$ electronic state cannot take place during the population transfer process, since the duration of the process is much shorter than the $A^1\Sigma_u^+$ lifetime. Note that the dynamics can be viewed as occurring entirely on the highest adiabatic time-dependent surface *if* the dynamics is adiabatic.

We solve the time-dependent Schrödinger equation, $i\hbar[\partial\Psi_j(R,t)/\partial t]=\Sigma_k\tilde{H}_{jk}(R,t)\Psi_k(R,t)$, using the Crank-Nicholson method [16]. Figure 2(a) shows the contour plots of the magnitude squared of the wave functions, $|\Psi_j(R,t)|^2$, $j=1,2,3$, as a function of time and space. Figure 2(b) shows the probability to be in the ith BO state, $\int dR|\Psi_i(R,t)|^2$ (solid curve), and the peak of the magnitude

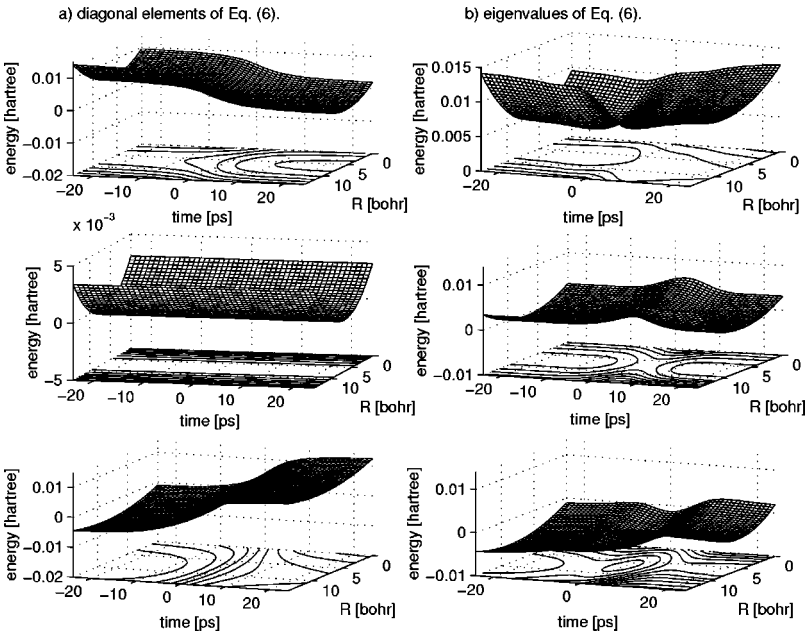

FIG. 1. (a) Diabatic time-dependent potentials [diagonal elements $\tilde{U}_{11}(R,t)$, $\tilde{U}_{22}(R,t)$ and $\tilde{U}_{33}(R,t)$ of Eq. (6)]. The chirps are responsible for the time variation of these surfaces. (b) Dressed-state time-dependent adiabatic surface potentials [eigenvalues of Eq. (6)].

of the wave packet, $\max_R[|\Psi_i(R,t)|^2]$ (dashed curve), versus time. The disappearance of $|\Psi_1(R,t)|^2$ over a narrow region of coordinate and time for which $\tilde{U}_{11}(R,t)$ and $\tilde{U}_{33}(R,t)$ intersect, in conjunction with the appearance of the wave packet in the $1\,^1\Pi_g$ BO state is clearly evident. Some transient population appears in the $A^1\Sigma_u^+$ state using our scheme, whereas in Garraway and Suominen's scheme no population of the second state results during the STIRAP process. However, since the pulse durations are short compared with the $A^1\Sigma_u^+$ decay time, no population is lost due to spontaneous emission during the process. At sufficiently large times, when no further population is transferred between electronic states, only the ground vibrational mode of the third electronic state is populated. The time-dependent wave packet does not oscillate in time as it would if a superposition of several modes were populated.

The results in Fig. 2 can be understood in terms of motion on the adiabatic surface correlating at early times with $X^1\Sigma_g^+$ and late times with the $1\,^1\Pi_g$ BO states. In order to ''engineer'' an adiabatic potential-energy surface upon which the population can evolve adiabatically from the initial to the final state, four control parameters are at our disposal: (1) the detunings Δ_ks, (2) the chirp rates $d\omega_k(t)/dt$, (3) the field strengths (peak Rabi frequencies $|\Omega_{k,max}|$), and (4) the pulse durations. These parameters were determined so that the motion of the wave packet is in fact adiabatic in the sense that the system wave packet (a) stays on the (highest) adiabatic surface and (b) remains as a ground vibrational wave packet on this surface during the dynamics. The determination of the field strengths, detunings, chirps, and pulse durations to accomplish this can be viewed as road design engineering of the time-dependent adiabatic surface in the top panel of Fig. 1(b). It contains features in the coupling region belonging to all three BO surfaces. Hence, it should not be surprising that all three BO states are populated during the process. Nevertheless, population does not remain in the $A^1\Sigma_u^+$ BO state because at late times the adiabatic surface correlates *only* with $1\,^1\Pi_g$ and does not contain any $A^1\Sigma_u^+$ (nor any $X^1\Sigma_g^+$) character.

The repulsion between the adiabatic states is proportional to the Rabi frequencies $|\Omega_{k,max}|$ when the $\tilde{U}_{11}(R,t)$ and $\tilde{U}_{33}(R,t)$ diabatic surfaces cross, which they do due to the chirps. Hence, choosing $|\Omega_{k,max}|$ too large can lead to a barrier on the upper surface (the relevant adiabatic surface). However, if the $|\Omega_{k,max}|$ are too weak, the couplings between the electronic states are turned off, a deep seam on the upper adiabatic time-dependent potential surface results wherein crosses the next highest adiabatic surface, and electronic and vibrational adiabaticity are not maintained. Figure 3 shows examples for such changes. The top panel in Fig. 3(a) replots the surface in Fig. 1, and the next two panels show the surfaces after being modified. In the middle panel the Rabi frequencies $\hbar|\Omega_{1,max}|=\hbar|\Omega_{2,max}|$ were decreased from 0.004 to 0.0004 hartree. The adiabatic surface exhibits a sharp seam in the coupling region where the first and third

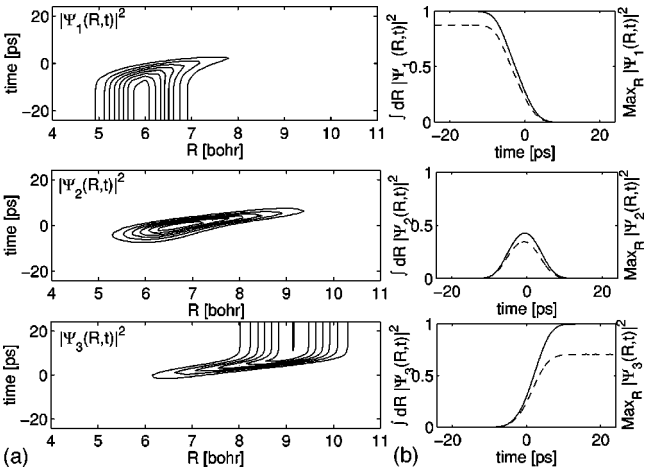

FIG. 2. (a) Contour plots of $|\Psi_i(R,t)|^2$, $i=1,2,3$ versus R and t. (b) $P_i(t)=\int dR|\Psi_i(R,t)|^2$ (solid curves) and $\max_R|\Psi_i(R,t)|^2$ (dashed curves) versus time.

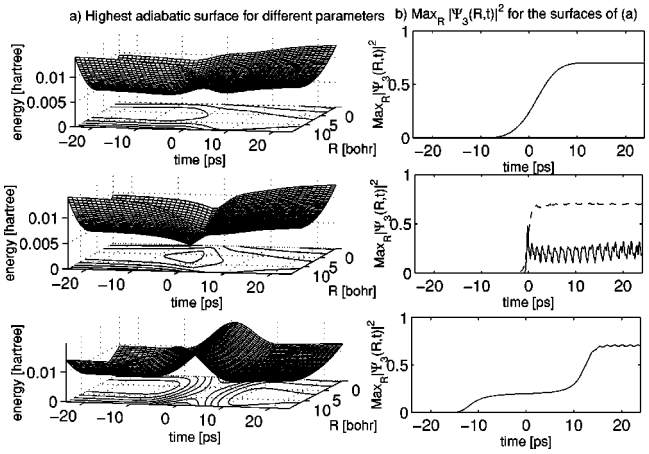

FIG. 3. (a) Highest time-dependent adiabatic surface. The upper panel is for the parameters used in Fig. 1; the middle and bottom panels have $\hbar\Omega_1=\hbar\Omega_2=0.0004$ and 0.01 hartree, respectively. (b) $\max_R[|\Psi_3(R,t)|^2]$ versus time corresponding to the parameters used to obtain the surfaces in (a). The dashed curve in the middle panel is for $\hbar\Omega_k=0.001$ hartree.

diagonal elements of $\tilde{\mathbf{U}}(R,t)$ in Eq. (6) intersect. The third panel shows the surface when $\hbar|\Omega_{1,max}|=\hbar|\Omega_{2,max}|$ are increased to 0.01 hartree. A strong repulsive barrier is now present due to the strong Rabi frequency coupling. The solid curves in Fig. 3(b) show the respective values of $\max_R[|\Psi_3(R,t)|^2]$. In the top panel, $\max_R[|\Psi_3(R,t)|^2]$ climbs smoothly to a maximum and no oscillations as a function of time are present after it reaches a maximum. This feature is consistent with a complete adiabatic transition as explained above [the expectation values $\langle\Psi_i(R,t)|R|\Psi_i(R,t)\rangle$ also vary smoothly with time]. In the lower two panels of Fig. 3(b), the curves depicting $\max_R|\Psi_3(R,t)|^2$ of the resulting wave packet exhibit wild oscillating time dependency (the solid and dashed curves in the middle panel correspond to a change of $\hbar|\Omega_{1,max}|=\hbar|\Omega_{2,max}|$ from 0.004 to 0.0004 and 0.001 hartree, respectively). This indicates nonadiabaticity, and reflects the admixing of higher vibrational components due to the nonsmooth adiabatic surface. The larger the deviation from smoothness of the surfaces, the larger the deviation from adiabaticity and admixing of higher vibrational levels. Nonadiabatic couplings result from off-diagonal matrix elements of the kinetic-energy operator. We are led to the following interpretation: when the adiabatic potential surface is not smooth enough or not sufficiently decoupled (far enough away) from the other adiabatic potentials, population can transfer between adiabatic surfaces and the final population can be distributed among several vibrational levels. Alternatively, if the coupling is too large and a potential barrier results on the adiabatic surface, nonadiabaticity can result. These features occur in the central and lower panels of Fig. 3.

To summarize and conclude, our ''road design engineering'' approach for choosing the desired parameters for constructing adiabatic light-induced potentials has led to the complete and adiabatic transfer of population from one vibronic state to another using picosecond-duration and GW/cm^2 intensity laser pulses. Hence, complete adiabatic transfer is obtained with reasonable laser intensities. This approach allows physically intuitive design concepts, such as the need to bank an S curve, to be used in the determination of the light pulses necessary for complete adiabatic population transfer. An extension of the road design approach to more than three electronic level systems may be possible, thereby generalizing previous results for transferring population of many-level systems by long-pulse sequences [11,12] to the short-pulse regime. Generalizations to more than one nuclear degree of freedom, as in polyatomic molecules, seem to be much more complicated; difficulties in visualization of the time-dependent potential-energy surface in E-t-$\mathbf{R}$ space hinder our ability to heuristically carry out the ''road design engineering.'' Our intuition will need to be further developed, and perhaps also coupled with auxiliary mathematical optimization methods.

This work was supported in part by grants from the James Franck Binational German-Israel Program in Laser-Matter Interaction and the National Science Foundation through a grant to the Institute for Theoretical Atomic and Molecular Physics at Harvard University and the Smithsonian Astrophysical Observatory.

[1] M. M. T. Loy, Phys. Rev. Lett. **32**, 814 (1974); **473**, 473 (1978).
[2] J. Oreg *et al.*, Phys. Rev. A **29**, 690 (1984); J. Oreg *et al.*, *ibid.* **32**, 2776 (1985).
[3] U. Gaubatz *et al.*, Chem. Phys. Lett. **149**, 463 (1988); J. Chem. Phys. **92**, 5363 (1990).
[4] Y. B. Band and P. S. Julienne, J. Chem. Phys. **94**, 5291 (1991); **95**, 5681 (1991).
[5] Y. B. Band, Phys. Rev. A **45**, 6643 (1992).
[6] Y. B. Band and P. S. Julienne, J. Chem. Phys. **96**, R3339 (1992).
[7] J. S. Melinger *et al.*, Phys. Rev. Lett. **68**, 2000 (1992).
[8] N. V. Vitanov and S. Stenholm, Phys. Rev. A **55**, 648 (1997).
[9] T. A. Laine and S. Stenholm, Phys. Rev. A **53**, 2501 (1996).
[10] C. E. Carroll and F. T. Hioe, Phys. Rev. A **42**, 1522 (1990).
[11] Y. B. Band, Phys. Rev. A **50**, 5046 (1994).
[12] Y. B. Band and O. Magnes, Phys. Rev. A **50**, 584 (1994).
[13] B. M. Garraway and K.-A. Suominen, Phys. Rev. Lett. **80**, 932 (1998).
[14] G. Herzberg, *Molecular Spectra and Molecular Structure: I. Spectra of Diatomic Molecules*, 2nd ed. (Van Nostrand, Princeton, NJ, 1950).
[15] T. Baumert *et al.*, Phys. Rev. Lett. **64**, 733 (1990); **67**, 3753 (1991); Chem. Phys. Lett. **191**, 639 (1992); **200**, 488 (1992); C. Meier and V. Engel, Phys. Rev. Lett. **73**, 3207 (1994); A. Assion *et al.*, Chem. Phys. Lett. **259**, 488 (1996); G. Jeung, J. Phys. B **16**, 4289 (1983).
[16] W. H. Press *et al.*, *Numerical Recipes* (Cambridge University Press, Cambridge, 1986), p. 635.